The effect of dynamic near-wake modulation on utility-scale wind turbine wake development

Aliza Abraham[1], **Luis A Martínez-Tossas**[2], **Jiarong Hong**[1,*]

[1]Department of Mechanical Engineering and St. Anthony Fall Laboratory, University of Minnesota, Minneapolis, MN 55455, USA
[2]National Renewable Energy Laboratory, Golden, CO 80401, USA

*Email: jhong@umn.edu

Abstract. High-resolution field-scale experiments using flow visualization with natural snowfall and high-fidelity large eddy simulations are combined to investigate the effect of dynamic turbine operation and atmospheric conditions on wind turbine wake mixing and recovery in the wake of a 2.5 MW wind turbine. Instantaneous near-wake expansion and deflection in response to changes in blade pitch and wind direction, termed dynamic wake modulation, is quantified using both techniques, demonstrating excellent agreement. The simulations are used to extend these results by calculating the energy flux into the wake 7 rotor diameters downstream, showing that dynamic turbine-atmospheric interactions enhance mixing in the far-wake. This finding is exhibited under both uniform and turbulent inflow conditions. Under turbulent flow, a synergistic relationship is also observed between dynamic wake modulation and wake meandering, as wake recovery can be further accelerated when the two phenomena occur together. The results of this study have implications for the development of more realistic far-wake models that include the significant impact of dynamic wake modulation on wake mixing and development. Additionally, the findings from the current study can be used to develop advanced control algorithms to speed up wake breakdown and recovery, further improving wind farm efficiency.

1. Introduction

Improved understanding of wind turbine wake development is required to mitigate the undesirable wake effects of power loss and increased fatigue loading on downwind turbines. In particular, wake recovery caused by re-entrainment of energy through mixing across the wake boundary is critical for increasing the amount of energy available to downwind turbines in a wind farm. It has been well established that several factors can influence wake recovery, including blade tip vortex breakdown [1], wind farm layout [2], and atmospheric stability [3]. Only recently, the effect of turbine operation on wake development has been investigated. Specifically, recent studies have proposed maximizing overall wind farm power by continuously regulating the thrust coefficient of each turbine, reducing the strength of the wake velocity deficit [4-7]. Two studies by Meyers and colleagues [8, 9] modelled in-line turbines with time-varying thrust coefficients to find the optimal time sequence for inducing wake breakdown before it reaches the downwind turbine. Another method of wake control is yaw steering, where a misalignment between the rotor and wind direction is applied to deflect the wake in the spanwise direction [10]. Though this method has achieved preliminary success in field tests on an operational wind farm [11],

some discrepancies have been observed between the predicted and observed wake deflection [12, 13]. These discrepancies suggest a lack of fundamental understanding of the mechanisms governing this behavior, likely caused by limitations of the techniques used to study it. Laboratory, numerical, and analytical methods must simplify turbine geometry, operational response, and/or atmospheric conditions to predict wake development. Field scale measurement techniques, meanwhile, lack sufficient spatiotemporal resolution to resolve coherent structures and instantaneous wake behavior.

To address the aforementioned limitations, Hong et al. [14] introduced super-large-scale flow visualization using natural snowfall to observe and quantify the flow in the wake of a utility-scale wind turbine. This technique provides high-resolution images of the wake with a field of view up to 100 m and has enabled the identification of several previously unobserved dynamic near-wake phenomena. Hong et al. [14] first characterized the relationship between the behavior of vortices shed from the blade tips and turbine operation. Dasari et al. [15] applied the technique to measure the flow over the entire vertical extent of the wake, identifying intermittent periods of wake contraction related to changes in blade pitch for the first time. Abraham et al. [16] investigated the effect of the tower and nacelle on the near-wake and the changes in their influence in response to changes in incoming flow. Most recently, Abraham and Hong [17] presented the first investigation into dynamic wake modulation, the large-scale motion of the wake in response to instantaneous changes in turbine operation and atmospheric conditions. Significantly, this study demonstrated the impact of dynamic wake modulation on mixing across the near-wake boundary and showed that it can contribute up to 20% more energy flux and an average of 11% more than that calculated without considering dynamic effects. The current study further investigates the impact of dynamic wake modulation on wake mixing and recovery by combining high-resolution field data with high-fidelity large eddy simulations (LES). The inclusion of LES enables the quantification of the wake behavior at multiple different planes simultaneously, particularly at distances farther downstream than those that can be captured in field-scale flow visualization experiments. Section 2 describes the experimental and LES methods in more detail, Section 3 presents the results of the investigations, and Section 4 summarizes the conclusions and provides a discussion of the results.

2. Methods

2.1. Experiment

The experimental portion of the study was conducted at the Eolos Wind Energy Research Field Station in Rosemount, MN. The site hosts a heavily instrumented 2.5 MW Clipper Liberty C96 wind turbine. The turbine is a three-bladed, horizontal-axis, pitch-regulated, variable speed machine with a 96 m rotor diameter (D) mounted atop an 80 m tall support tower (H_{hub}). The area surrounding the turbine is primarily flat farmland, harvested at the time, with short vegetation covered over with snow. The experiment took place between 19:00 and 22:00 CST on January 22nd, 2018, at night during a snowstorm, indicating a neutral boundary layer. The incoming wind speed varied significantly over the course of the experiment, with instantaneous values between 2 m/s and 17 m/s at the hub, allowing the characterization of the wake under different turbine regions of operation. The wind direction also varied between approximately −30° and 20° clockwise from north. During the experiment, a light sheet was used to illuminate the snowflakes in a plane parallel to the rotor (perpendicular to the flow) 17 m (0.2D) downstream of the turbine (figure 1a). A camera captured images of the snowflakes within the light sheet with a field of view of 73 m × 129 m (spanwise × vertical) for more than 2 h (sample enhanced image in figure 1b). Coherent vortex structures in the flow appear as voids in the snow particle seeding projected onto the light sheet due to the centrifugal effect on the inertial particles caused by the strongly rotating fluid [15]. The vortices shed from the blade tips were used to identify the outer wake boundary, and the portion of this helix above the hub (and therefore unaffected by the tower wake) was fit with an envelope to capture the overall shape and motion of the whole wake (figure 1c). Cross-sections of this envelope were compared to the boundary of the wake with no expansion or deflection included (referred to as the model wake), extracted from a SolidWorks model of the experimental setup. The deformation of the envelope relative to the model wake was used to quantify the dynamic wake modulation including

deflection, $\delta_{w,y}$, and expansion, $\delta_{w,z}$. The displacements $\delta_{w,y}$ and $\delta_{w,z}$ were converted to angles, ξ and φ respectively, using the distance between the light sheet and the turbine (see [17] for more details).

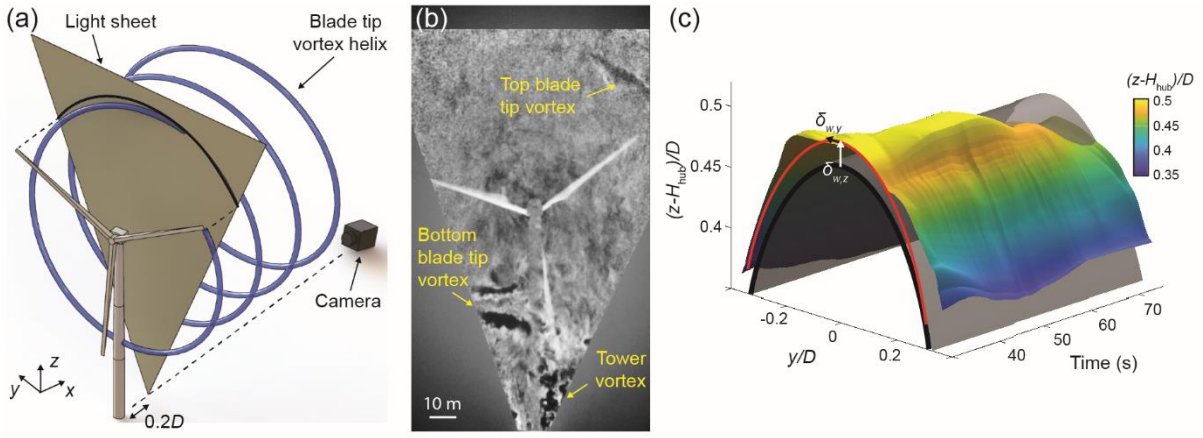

Figure 1. (a) Schematic of the experimental setup of the field study, including the turbine, light sheet, and camera. The blue helix represents the blade tip vortex and the black line indicates the location of the intersection between the model wake and light sheet. The origin of the coordinate system is at the base of the turbine support tower. (b) Sample snow particle image, with vortices shed from the blade tips and towers indicated in yellow. The image is enhanced to make the coherent structures (appearing as dark voids) easier to see. (c) Sample time series of the wake envelope (colored surface) compared to the model wake (gray surface). Figure adapted from [17].

2.2. Simulations

To develop further understanding of this phenomenon and to isolate the effect of individual parameters, large eddy simulations (LES) of the Eolos turbine and its wake were conducted. The simulations were performed with Nalu-Wind, a wind-focused fork of the incompressible flow solver developed by Sandia National Laboratories, Nalu [18]. A model of the turbine was developed in OpenFAST and incorporated into the LES using actuator lines [19]. To isolate the influence of dynamic wake modulation associated with changing turbine operation and incoming flow conditions, the simulations were first conducted using uniform laminar inflow with a wind speed of 10 m/s. The changing turbine operation was implemented by modifying the turbine controller with a hard-coded time series of pitch rates, as blade pitch was shown to be one of the main contributors to changes in wake expansion and contraction [15, 17]. The blade pitch was varied linearly at 5 different rates, for 10 seconds each in the positive and negative directions (figure 2a). The rotor speed started at 14.7 RPM but was allowed to change in response to changes in blade pitch. Changing incoming flow conditions were modelled by sinusoidally varying the wind direction with increasing magnitude (maximum of 20°, figure 2b) while the rotor yaw angle was held constant. These time series were selected to approximately match the magnitudes and rates of change of the blade pitch and wind direction from the field experiment in a more organized and controlled pattern than that observed in the field.

Simulations with turbulent inflow were performed next to explore the effects of dynamic wake modulation under more realistic conditions. The turbulent flow was generated in a 2500 m × 2500 m × 500 m volume using a precursor simulation with periodic boundary conditions in the streamwise and spanwise directions. The top surface was capped with an inversion layer and a shear stress boundary condition was applied to the bottom surface using the logarithmic law for rough walls with a friction velocity of $u^* = 0.95$ m/s and a roughness length of $z_0 = 0.53$ m. The turbulence was allowed to develop for 20000 s in order to reach a quasi-steady equilibrium state. Then the simulation was run for another 2000 s to generate a fully developed turbulent inflow boundary condition for the turbine simulation.

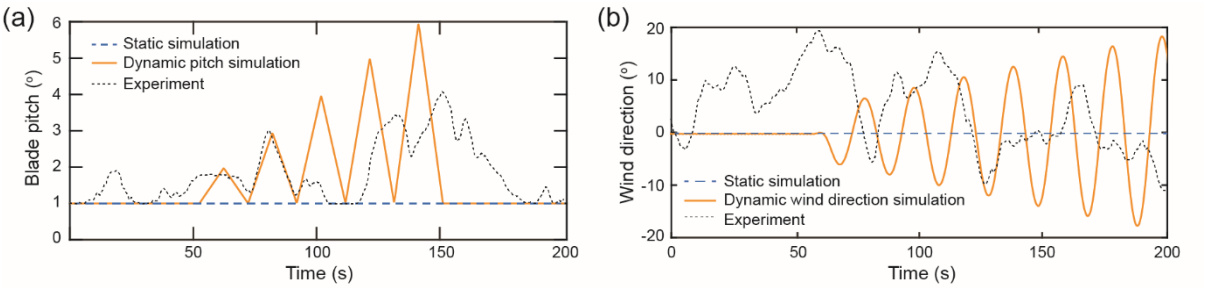

Figure 2. Time series of (a) blade pitch and (b) wind direction for the static and dynamic simulations compared to a sample time sequence from the field experiment.

3. Results

3.1 Near wake modulation

First, the uniform flow simulations are used to compare the effect of pitch changes on the near wake to that observed in the field study. The instantaneous expansion of the wake at $0.2D$ downstream is compared between the experiment and simulations in figure 3(a). In the experimental data, the expansion is defined using the difference between the wake envelope and the model wake [17]. In the simulation, expansion is calculated by fitting a two-dimensional Gaussian function to the velocity deficit:

$$u_\infty - u(y,z) = A * \exp\left(-\frac{(y-y_c)^2+(z-z_c)^2}{2\sigma^2}\right),$$

where (y_c, z_c) is center of the Gaussian, σ^2 is the variance, and A is a fitting coefficient. Both the field study and the simulation show a clear inverse correlation between the wake expansion and the blade pitch. Such correlation is associated with the reduction in lift along the blades when the pitch increases (angle of attack decreases), and the corresponding reduction in thrust coefficient. Moreover, the slope and spread of the experimental and simulated data correspond reasonably well, suggesting the simplified simulation successfully captures the effect of changes in blade pitch on dynamic wake modulation. Note that the controller was not modified in the field experiment; rather the pitch changes already implemented by the turbine operating above the rated wind speed caused the observed changes in wake expansion.

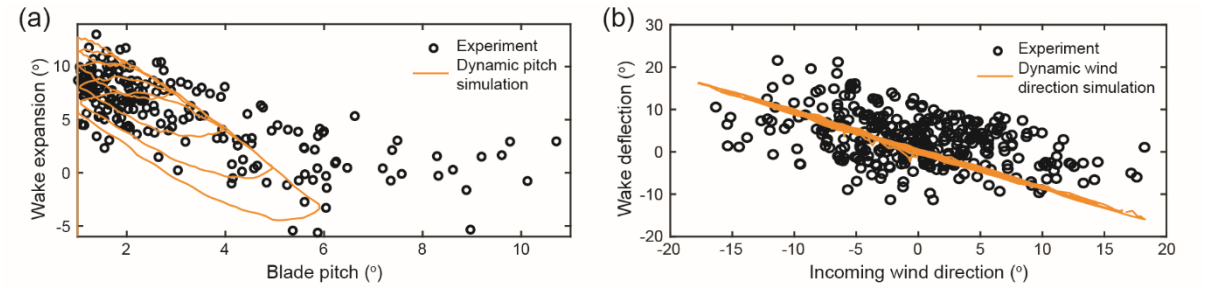

Figure 3. Comparison of (a) dynamic wake expansion and (b) spanwise wake deflection in the experiment from [17] and the dynamic simulations in the near wake at $0.2D$ downstream.

Next the effect of wind direction changes on the instantaneous spanwise deflection of the near wake is compared to the field study in figure 3(b). Again, the trends observed in the experiment and simulation align well, both exhibiting an inverse relationship between wind direction and instantaneous wake deflection. Interestingly, this trend is opposite to that observed during steady wind direction misalignment (e.g., [10]). As described in Abraham and Hong [17], this opposite deflection is related to the timescale of the wind direction changes. Spanwise wake deflection takes time to stabilize under sudden changes in wind direction, so constant changes (like those experienced by turbines in the field

and those modelled here) can cause significant disturbance to the process of the wake transitioning to the fully deflected state it experiences when the wind direction is steady. Note that the simulation data exhibits significantly less spread than the experimental data, as the timescale is consistent in the simulation but highly variable in the field.

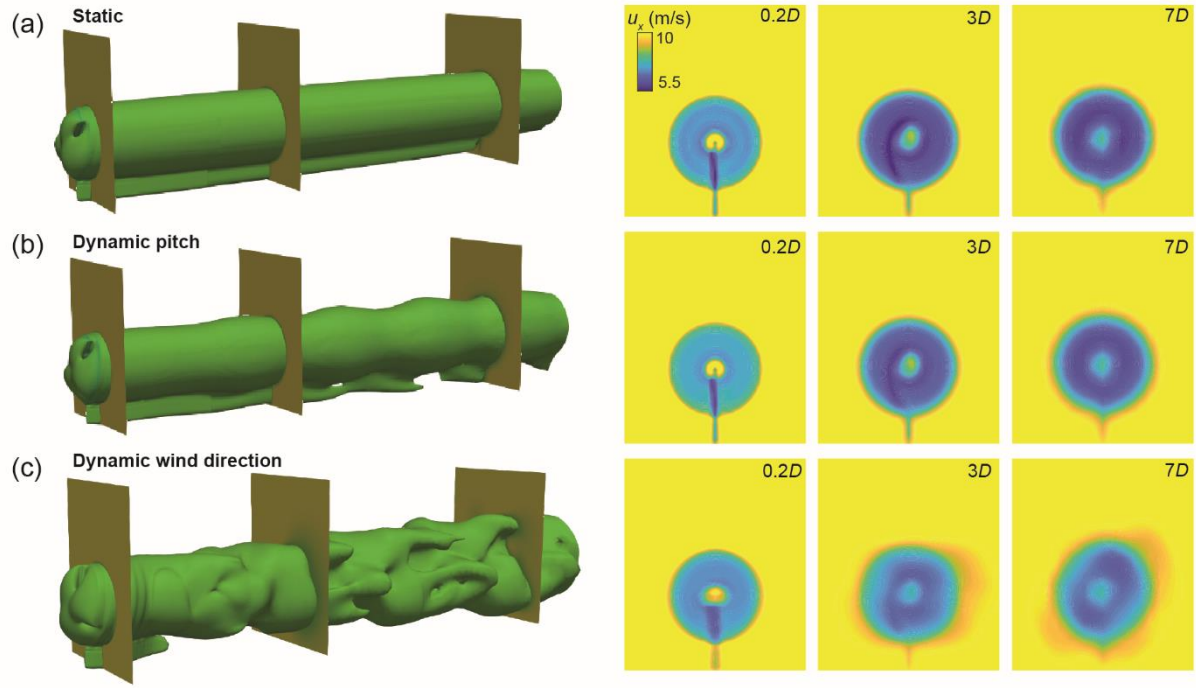

Figure 4. Sample instantaneous isocontours of velocity ($u_x = 9$ m/s) from (a) the static uniform inflow simulation, (b) the dynamic pitch uniform inflow simulation, and (c) the dynamic wind direction uniform inflow simulation with cross-sections showing mean streamwise velocity at three downstream locations.

3.2. Far wake mixing under uniform flow

Figure 4 shows the wake under the three uniform flow conditions, with cross-sections showing the mean streamwise velocity at three downstream distances. Both dynamic cases show accelerated wake recovery compared to the static case, indicated by the increased spread and reduced magnitude of the velocity deficit. These features are clearest at the farthest downstream distance (7*D*), but can also be observed closer to the turbine. The dynamic cases also exhibit deformed wake boundaries, indicating that the boundary deformation is intrinsically related to the accelerated wake recovery. This connection is particularly clear in the dynamic wind direction case where the wake boundary is significantly disturbed and the velocity deficit reduction is the strongest.

The accelerated wake recovery is caused by enhanced energy flux into the wake, quantified in figure 5 for both dynamic cases at 7*D* downstream (the typical turbine spacing in current wind farms [20]). The energy flux per unit length, calculated as $\Phi = \overline{u_x}\langle u'_x u'_r \rangle_{r=D/2}$, increases with the magnitude of the pitch changes and wind direction changes, as they cause fluctuations in the wake boundary that enhance the mixing across the boundary. The energy flux from the dynamic cases is compared to that from the static case, where it stays constant near zero (no turbulent mixing occurs in this uniform flow simulation).

3.3. Far wake mixing under turbulent flow

Dynamic wake modulation is next simulated with turbulent inflow to obtain a more realistic understanding of how this modulation affects wake mixing in the atmospheric conditions experienced by utility-scale turbines. With the turbulent inflow, only dynamic pitch is simulated, as the stochasticity

of the atmospheric wind direction cannot be readily incorporated into the turbulent simulation at this point. The same blade pitch sequence used in the uniform flow simulation (figure 2a) is applied here. Figure 6 compares the wake in the static and dynamic pitch cases. It is immediately apparent that the turbulent inflow substantially deforms the wake boundary and enhances mixing compared to the uniform inflow case, accelerating wake recovery. By the time the wake reaches $7D$ downstream, significant recovery has occurred in both the static and dynamic pitch cases. However, some differences between the two cases can still be observed. In the $3D$ and $7D$ planes, the velocity deficit is slightly weaker for the dynamic pitch case than the static pitch case. This finding suggests that dynamic wake modulation still enhances mixing, even under the high-flux conditions of turbulent inflow.

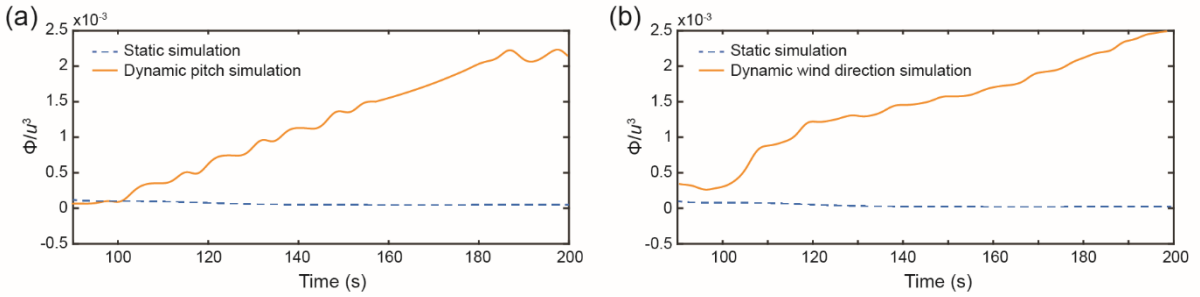

Figure 5. (a) Energy flux per unit length into the wake for the static uniform flow simulation and the dynamic pitch uniform flow simulation. (b) Energy flux per unit length into the wake for the static uniform flow simulation and the dynamic wind direction uniform flow simulation. Note that the delay in the start of the signal is due to wake propagation time.

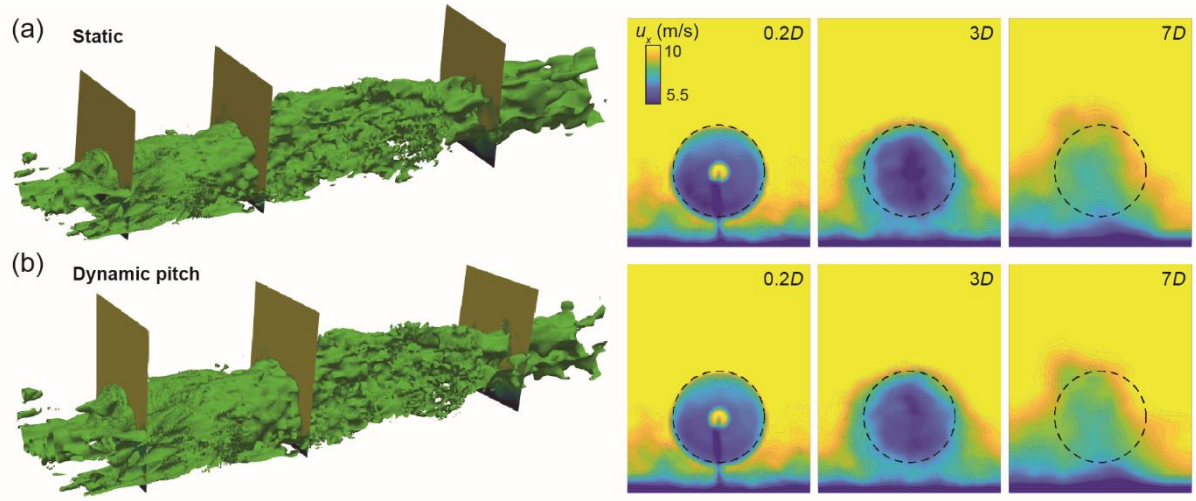

Figure 6. Sample instantaneous isocontours of velocity ($u_x = 9\ \mathrm{m/s}$) from (a) the static turbulent inflow simulation and (b) the dynamic pitch turbulent inflow simulation with cross-sections showing mean streamwise velocity at three downstream locations. The dashed circle indicates the rotor position.

The aforementioned effect is again quantified using the energy flux at the wake boundary $7D$ downstream, shown in figure 7 for the static and dynamic pitch cases. Though the magnitudes are much closer than in the uniform flow cases, dynamic pitch still enhances mixing across the boundary by an average of 12%. This value is comparable to that reported in the experimental study for the estimated effect of dynamic wake modulation on energy flux in the near wake [17]. Significantly, the pitch changes modelled in the current study are on the same order as those that occur during normal above-rated turbine

operation (as demonstrated in figure 2a), so the observed enhanced mixing is already occurring frequently in the wake of utility-scale turbines.

Figure 7 also shows that the flux enhancement is not constant. There is even a period where the dynamic pitch case exhibits a lower flux than the static pitch case. The intermittency of the flux enhancement suggests that the dynamic wake modulation may be interacting with another unsteady process in the far-wake, i.e., wake meandering. Figure 8 provides further support for this interpretation, comparing top-view cross-sections of the static and dynamic pitch cases at two time points. The first time point (figures 8a and b) provides an explanation for the decreased flux observed in the dynamic pitch case. At ~6*D* downstream, a region of the dynamic pitch wake has an increased velocity deficit compared to the static pitch wake, though the inflow in both cases is the same. This observation suggests wake meandering and dynamic wake modulation have a destructive relationship at that moment, inhibiting wake mixing and breakdown. However, throughout most of the simulation these two phenomena appear to have a constructive relationship, working together to enhance mixing. A second time point is shown in figures 8(c) and (d), where the wake exhibits a turn at ~5*D* downstream, indicated by the white arrow in the figure. At this point, the velocity deficit is significantly lower in the dynamic pitching case than in the static pitching case, suggesting dynamic wake modulation augments the mixing caused by meandering. This constructive relationship likely occurs most of the time, as the average mixing during the dynamic pitch simulation is higher than that in the static pitch simulation.

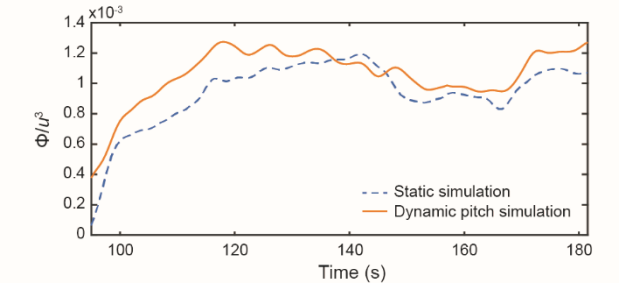

Figure 7. Energy flux per unit length into the wake for the static turbulent flow simulation and the dynamic pitch turbulent flow simulation.

4. Conclusions and discussion

High-fidelity LES was combined with field scale experiments to investigate the effect of dynamic turbine operation and atmospheric conditions on mixing and recovery in the wake of a 2.5 MW wind turbine. The novel high-resolution flow visualization technique using natural snowfall enabled the quantification of instantaneous near-wake expansion and deflection, termed dynamic wake modulation, in response to changes in blade pitch and wind direction. Simulations were performed to isolate these variables, and the same trends as those observed in the experiments were revealed. Further, energy flux into the wake 7*D* downstream was calculated, showing dynamic turbine-atmospheric interactions enhance mixing in the far-wake. This finding was demonstrated under both uniform and turbulent inflow conditions. Under turbulent flow, a synergistic relationship was observed between dynamic wake modulation and wake meandering, as wake recovery was further accelerated when the two phenomena occurred together.

The current study is limited to neutrally stable atmospheric conditions because of the restrictive weather conditions under which the flow visualization experiments can take place (i.e., during snowstorms). In future studies, additional atmospheric stabilities will be investigated using simulations to understand the effect of this variable on the enhanced mixing caused by dynamic wake modulation. Furthermore, we were unable to simulate the large-scale changes in wind speed and direction that occur in the atmosphere. Though this atmospheric stochasticity is a crucial aspect of dynamic wake modulation, it is notoriously difficult to model in simulations [21]. One way to address this limitation would be to couple atmospheric flow simulations at different scales (e.g., mesoscale and microscale), an avenue which will be explored in future studies.

The results of the current study can be applied to the development of more realistic far-wake models. Currently, dynamic wake modulation is not considered in conventional wake models, though we have demonstrated here that it can have a significant impact on wake mixing and development. Improved wake models will allow wind farm layouts to be designed more efficiently, reducing the levelized cost of wind energy. Additionally, the findings from the current study can be used to develop advanced control algorithms to speed up wake breakdown and recovery, further improving wind farm efficiency.

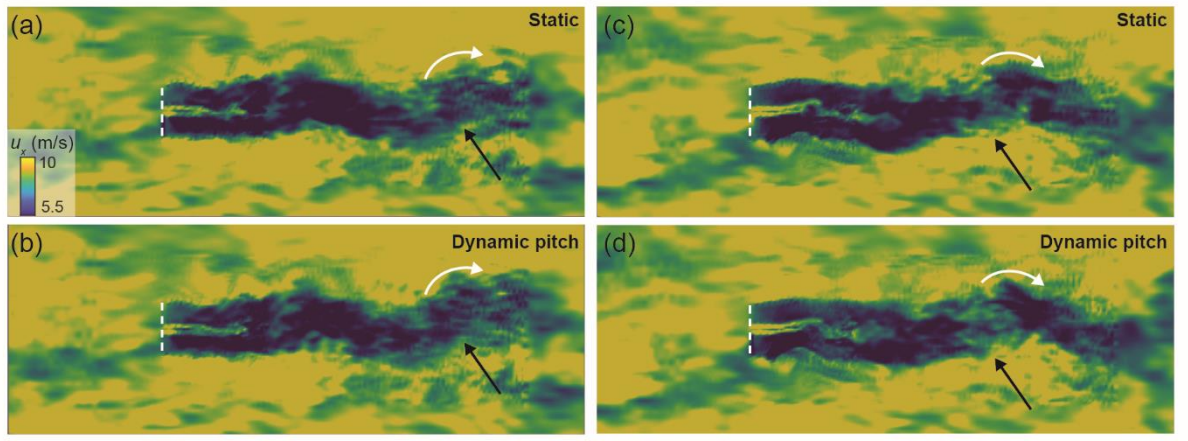

Figure 8. Interaction between dynamic wake modulation and meandering in turbulent flow. Sample streamwise velocity field at plane $z = H_{\mathrm{hub}}$ during the same instant for the (a) static pitch simulation and (b) dynamic pitch simulation. Sample streamwise velocity field at plane $z = H_{\mathrm{hub}}$ during a second time for the (c) static pitch simulation and (d) dynamic pitch simulation. The dashed white line indicates the position of the rotor and the black arrow points to the location where a significant difference in velocity deficit between the two cases can be observed. The white curved arrow highlights the turning motion of the wake due to meandering.

References

[1] Lignarolo LEM, Ragni D, Scarano F, Simão Ferreira CJ and Van Bussel GJW 2015 *J. Fluid Mech.* **781** 467-93
[2] Vermeer L, Sørensen J and Crespo A 2003 *Prog. Aerosp. Sci.* **39** 467-510
[3] Hansen KS, Barthelmie RJ, Jensen LE and Sommer A 2012 *Wind Energy* **15** 183-96
[4] Corten GP and Schaak P 2003 *Proc. EWEC 2003, Madrid*
[5] Marden JR, Ruben SD and Pao LY 2013 *IEEE Trans. Control Syst. Technol*. **21** 1207-14
[6] Gebraad PMO and van Wingerden JW 2014 *Wind Energy* **18** 429-47
[7] Goit JP and Meyers J 2015 *J. Fluid Mech.* **768** 5-50
[8] Munters W and Meyers J 2018 *Wind Energy Sci.* **3** 409-25
[9] Yilmaz A and Meyers J 2018 *Phys. Fluids* **30** 085106
[10] Jiménez Á, Crespo A and Migoya E 2010 *Wind Energy* **13** 559-72
[11] Howland MF, Lele SK and Dabiri JO 2019 *Proc. Natl. Acad. Sci. U.S.A*. **116** 14495-500
[12] Trujillo J, Bingöl F, Larsen GC, Mann J and Kühn M 2011 *Wind Energy* **14** 61-75
[13] Larsen TJ, Madsen HA, Larsen GC and Hansen KS 2013 *Wind Energy* **16** 605-24
[14] Hong J, Toloui M, Chamorro LP, Guala M, Howard K, Riley S, Tucker J and Sotiropoulos F 2014 *Nat. Commun*. **5** 4216
[15] Dasari T, Wu Y, Liu Y and Hong J 2019 *J. Fluid Mech.* **859** 204-46
[16] Abraham A, Dasari T and Hong J 2019 *J. Wind Eng. Indust. Aerodyn*. **193** 103981
[17] Abraham A and Hong J 2020 *Appl. Energy* **257** 114003
[18] Sprague MA, Ananthan S, Vijayakumar G and Robinson M 2020 *J. Phys.: Conf. Ser.* **1452**

012071
[19] Sørensen JN and Shen WZ 2002 *J. Fluids Eng.* **124** 393-399
[20] Meyers J and Meneveau C 2012 *Wind Energy* **15** 305-17
[21] Veers P, *et al*. 2019 *Science* **366** eaau2027